ISTITUTO NAZIONALE DI FISICA NUCLEARE

Sezione di Trieste

INFN/BE-92/06

27 agosto 1992

Edoardo Milotti

RADIATIVE TRANSITIONS IN MUONIC HYDROGEN

Servizio Documentazione
dei Laboratori Nazionali di Frascati

RADIATIVE TRANSITIONS IN MUONIC HYDROGEN

Edoardo Milotti

Dipartimento di Fisica dell'Università di Trieste
and
Istituto Nazionale di Fisica Nucleare
Sezione di Trieste, Via Valerio 2, I-34127 Trieste, Italy

Abstract

Recently a new experimental proposal has been put forward to observe and measure the level shifts in muonic hydrogen. Extensive calculations have been carried out in the frame of this experiment to find out the most suitable transitions. This note reports the results of these calculations.

1. Introduction

The splittings of the atomic energy levels of muonic hydrogen - i.e. the μ-p bound system - are largely due to the polarization of QED vacuum with electron-positron loops, therefore a measurement of these splittings provides an accurate test of QED.

It is not possible to measure the splittings with a spectroscopic instrument, since a resolution $\frac{\lambda}{\delta\lambda} \approx 10^4 \div 10^6$ in the soft X-ray domain would be required just to detect them. For this reason there have been attempts to measure the splittings with the double resonance method [1]. However one needs an exceedingly powerful far-infrared (FIR) source to induce the transitions and those experiments did not reach their initial goals. Recently, new powerful electromagnetic radiation sources have become available, and a new experimental proposal has been put forward [2]. Extensive calculations have been carried out in the frame of this experiment to find the most suitable transitions. This note reports the results of these calculations.

All the calculations have been carried out with the Schrödinger wavefunctions and using first-order perturbation theory only; more exact calculations exist [3], but they are not always readily available or so extensive as needed. The values of the physical constants that are needed at some point of the procedure are given in table 1 [4].

The binding energies from the simple Balmer formula up to n=14 are given in table 2. I stopped at n=14 because at this n the average radii of the radial muonic wavefunction and of the electronic wavefunction coincide, and detailed Monte Carlo calculations confirm that the muons are captured at n≈14 [5]. Moreover when a muon is captured in a hydrogen gas target it can be shown that Stark mixing due to collisions with the neighbouring molecules is more probable than the radiative transitions for n>5 at low pressures [6], therefore all the other listings in this note stop at n=5.

2. Lifetimes

The radiative transition probabilities per unit time for transitions (n,l) -> (n',l±1) have been calculated numerically from the formulas of paragraph 59 of ref. [7], and are listed in table 3. These are the transition probabilities for the electric dipole matrix element, and account nearly for the whole width of each level. Thus the lifetime τ of a certain level is given by

$$\frac{1}{\tau} \approx \Gamma_1 + \Gamma_2 + \ldots = \Gamma \qquad (1)$$

where the Γ_i's are the transition probabilities per unit time for the transitions (n,l) -> (n',l±1) associated to that level, and Γ is its width. These lifetimes are listed in table 4. Table 3 lists also the intensity of each line obtained as the product $\hbar n_i \Gamma_i$ (see [7]).

3. Level shifts

The realization that muonic atoms may provide useful insights is an old one, and the theoretical calculations that were scattered in several papers have been collected in the excellent review paper by Borie and Rinker [3]. I have used the formulas in this paper to compute the QED corrections, while for the fine structure and hyperfine structure corrections I have used the formulas in [7].

Neglecting the proton electromagnetic structure, and using the notation of [3], the Ühling-Serber potential [8,3] is given by

$$V_{VP1}(r) = -\frac{2\alpha}{3\pi}\frac{Z\alpha}{r}\chi_1(2m_e r) \qquad (2)$$

where

$$\chi_1(x) = \int_1^\infty dz\, \frac{\sqrt{z^2-1}}{z^2}\left(1+\frac{1}{2z^2}\right)e^{-xz} \qquad (3)$$

I have computed numerically the function $\chi_1(x)$, and I have then used the potential (2) to find the order-α QED level shifts from first-order perturbation theory.

For the Källen-Sabry potential I have taken the asymptotic expression for large r [3]:

$$V_{VP2}(r) \approx \alpha^2 \frac{Z\alpha}{r}\frac{e^{-2m_e r}}{m_e r}\left(\frac{8}{\pi^2}\log^2 2 - \frac{1}{4}\right) \qquad (4)$$

and again I have applied first-order perturbation theory to find the resulting order-α^2 shift.

The numerical results for these four corrections are listed in tables 5 and 6.

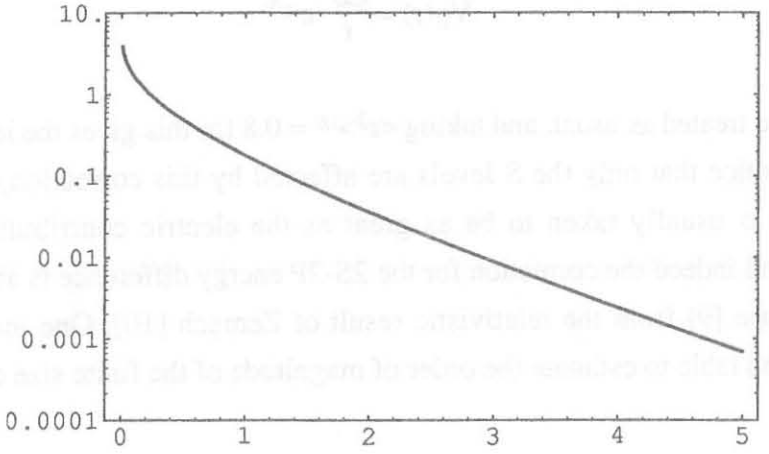

Figure 1: Plot of $\chi_1(x)$ vs. x.

4. Other corrections

There are some other corrections that have not been included in the calculation of the level shifts, since they are very much smaller than those included, and probably smaller than the "procedural errors" (there are several such "errors", due to the rough approximations in the calculations: the wavefunctions are Schrödinger wavefunctions instead of Dirac wavefunctions, I have used first order perturbation theory, etc. Indeed the numbers listed in table 5 for the 2S-2P transitions are ~10% higher than those given in [9]). I wish only to mention the correction due the proton finite size that can be discussed, at least qualitatively, in simple terms. Since the proton is not point-like it has both an electric and a magnetic form factor, and the correction due to the electric form factor is very easy to compute in the framework of non-relativistic perturbation theory. If one assumes that the electric charge density of the proton has the exponential shape

$$\rho(r) = \left(\frac{3}{\langle r^2\rangle^{1/2}}\right)^{3/2} \exp\left(\frac{-2\sqrt{3}\, r}{\langle r^2\rangle^{1/2}}\right) \qquad (5)$$

where $\langle r^2\rangle^{1/2}$ is the proton rms radius, then the Coulomb potential changes to

$$V(r) = -\frac{Ze^2}{r}(1 - e^{-r/R}) \qquad \text{(c.g.s. units)} \qquad (6)$$

with $R = \frac{\langle r^2\rangle^{1/2}}{2\sqrt{3}}$. Therefore the charge spread produces a perturbing potential

$$V_{ff}(r) = \frac{Ze^2}{r} e^{-r/R} \qquad (7)$$

which may be treated as usual, and taking $\langle r^2 \rangle^{1/2} = 0.8$ fm this gives the level shifts listed in table 7 (notice that only the S levels are affected by this correction). The magnetic contribution is usually taken to be as great as the electric contribution to the total correction, and indeed the correction for the 2S-2P energy difference is about half of that found by Borie [9] from the relativistic result of Zemach [10]. One may thus use the numbers in the table to estimate the order of magnitude of the finite size corrections also for higher n.

5. The (n,l)->(n,l±1) transition probabilities

The electric dipole (n,l)->(n,l±1) transition probabilities per unit time must be evaluated to find the "best" transitions for the double resonance method.

Quantum-mechanically one should describe the stimulated transition between two levels of the μp system with the formalism used for lasers with more than two levels [11]. However it is also possible to use the simple Fermi Golden Rule, and it has been shown that the exact results coincide with the Golden Rule results for long pulses in the double resonance method [12].

The Golden Rule expression for the transition probability per unit time is

$$T_{if}(\omega) = \frac{e^2 Z_0}{2h^2} f_i \frac{\Gamma/\Gamma_i}{(\omega_o-\omega)^2+\Gamma^2/4} \left[\bar{\sum} |\langle \Psi_f | r \cos\theta | \Psi_i \rangle|^2 \right] \overline{I}, \qquad (8)$$

where Z_0 is the impedance of vacuum ($\approx 377\ \Omega$); $\overline{I}$ is the average intensity of radiation on muonic hydrogen in W/m^2; f_i is the statistical population of the initial level (this will be discussed in the next section); Γ_i, Γ_f are the widths of the initial and final level and $\Gamma = \Gamma_i + \Gamma_f$; $h\omega_o$ is the energy difference between initial and final level and the sum is performed over all the final states and averaged over all the initial states. The total transition probability per unit time must include also the possibility of a reversed transition, so that

$$T(\omega) = T_{if}(\omega) - T_{fi}(\omega) . \qquad (9)$$

The terms of the averaged sum can be separately evaluated for the radial and the angular part. The radial part is easy: since only |D|| = 1 transitions are allowed, one can use the exact expression [7]:

$$|\langle f| r |i\rangle| = \frac{3}{2} n \sqrt{n^2 - l^2}\ a_\mu \qquad (10)$$

for transitions (n,l) -> (n,l±1), where a_μ is the Bohr radius for muonic hydrogen ($a_\mu \approx 2.85\ 10^{13}$ m). The angular part is more difficult: it involves linear combinations of several spherical harmonics and requires many Clebsch-Gordan coefficients.

These calculations have been carried out for the transitions 4P-4D, 3P-3D and 4S-4P, and the values $\frac{T_{max}}{\overline{I}} = \frac{T(\omega_0)}{\overline{I}}$ are listed in table 8. The notation used for the levels is nL_j^{2f+1}. The listing includes only the transitions allowed by the selection rules:

$$\begin{aligned} &|\Delta l| = 1; \\ &|\Delta j| \le 1; \\ &|\Delta f| \le 1; \quad (f = 0) \leftrightarrow (f = 0) \text{ forbidden} \end{aligned} \qquad (10)$$

Moreover, using these transition probabilities and the level shifts discussed in section 3, it is possible to plot the "absorption spectra" for the various hyperfine lines corresponding to these transitions. The spectra are shown in figures 2,3 and 4; the vertical scale is in arbitrary units, and is the same for the three plots.

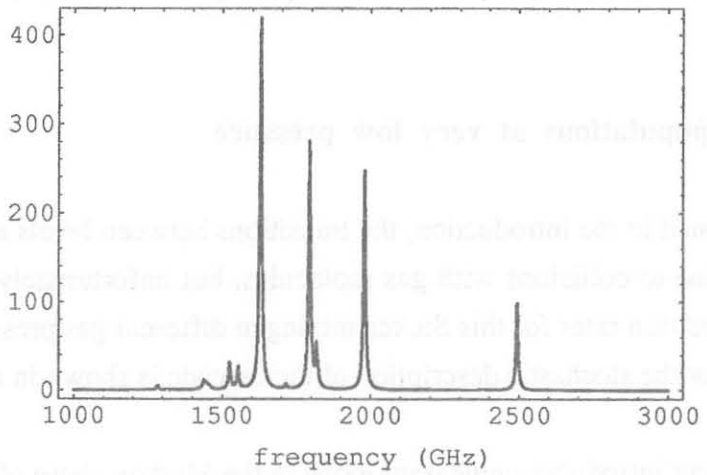

Figure 2: T(ω) (arbitrary units) vs. frequency for the 3D-3P transition

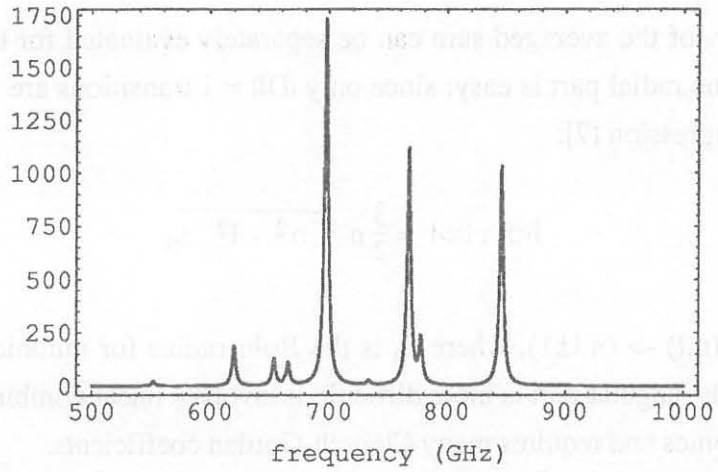

Figure 3: T(ω) (arbitrary units) vs. frequency for the 4D-4P transition

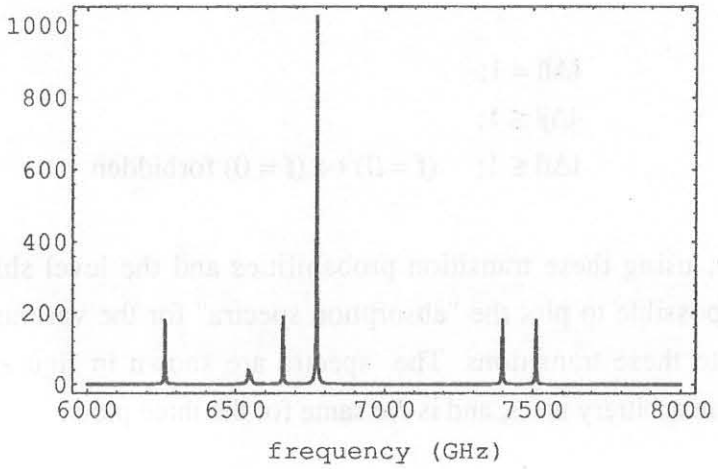

Figure 4: T(ω) (arbitrary units) vs. frequency for the 4S-4P transition

6. Statistical populations at very low pressure

As mentioned in the introduction, the transitions between levels are influenced by Stark mixing, due to collisions with gas molecules, but unfortunately it is difficult to evaluate the transition rates for this Stokes mixing at different gas pressures. A (partial) Markov chain for the stochastic description of the cascade is shown in figure 5 (see also [6]).

Stark mixing introduces unpleasant loops in the Markov chain of the cascade and this makes an analytical evaluation of the populations impractical. However, if one

neglects the Stark mixing it is straightforward to calculate the statistical populations of the different levels from the transition probabilities per unit time Γ_i defined in section 2. Stark mixing becomes negligible at very low gas pressures (<30 mbar) [6] for n < 6: thus one can assume that the population of initial muons is uniformly distributed for n=6 with all the available l,m values. Thereafter each state i decays to one of the reachable states f with a conditional probability

$$B_{if} = \frac{\Gamma_f}{\Gamma(i)} \tag{10}$$

where $\Gamma(i)$ is the total width of state i.

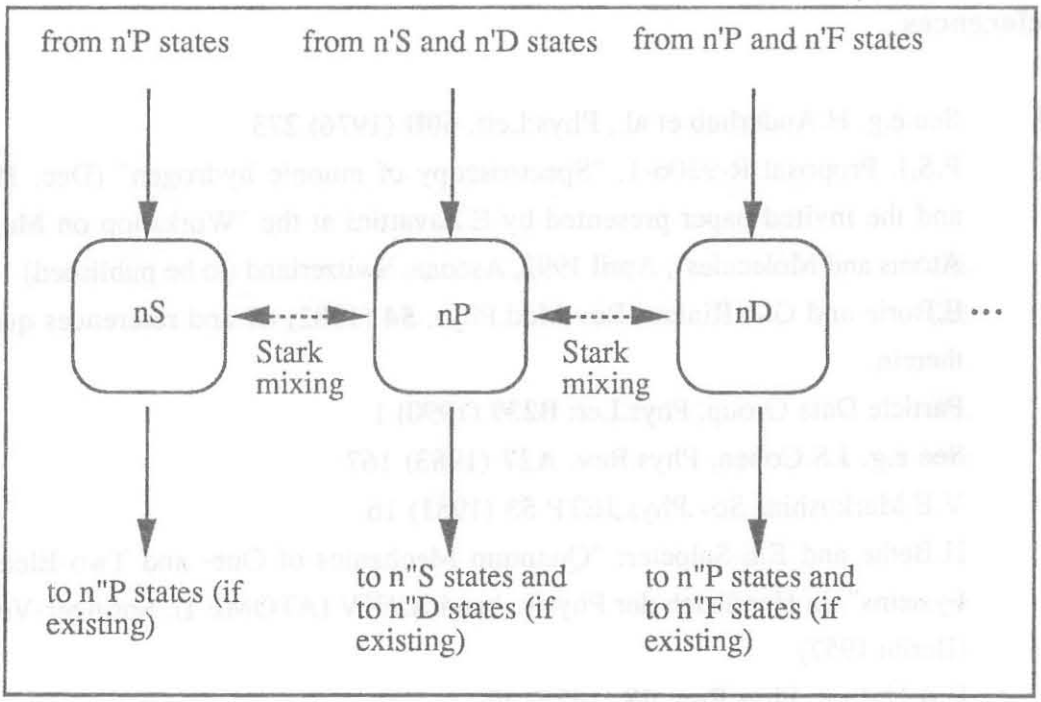

Figure 5: Partial Markov chain description of the cascade

Therefore, if a state f can be reached from several states i, and each state i has a probability p_i of being occupied by a muon, the probability p_f that the level f is occupied by a muon at some time during the cascade is:

$$p_f = \sum_{\{i\}} p_i \, B_{if} \tag{11}$$

The results of this simplified calculation are listed in table 9, and they are in good agreement with a Monte Carlo code developed by Borie and Leon [13].

Still another statistical factor must be included when dealing with the hyperfine components of each line: then if one assumes a uniform distribution among the hyperfine sublevels, the relative abundances in each sublevel are those given in table 10.

Acknowledgement

I wish to thank Prof. E. Zavattini, who is the real originator of the experimental project [2], for the fruitful discussions and advice.

References

[1] See e.g. H.Anderhub et al., Phys.Lett. **60B** (1976) 273

[2] P.S.I. Proposal R-9206-1, "Spectroscopy of muonic hydrogen" (Dec. 1991) and the invited paper presented by E.Zavattini at the "Workshop on Muonic Atoms and Molecules", April 1992, Ascona, Switzerland (to be published)

[3] E.Borie and G.A.Rinker, Rev.Mod.Phys. **54** (1982) 67 and references quoted therein.

[4] Particle Data Group, Phys.Lett **B239** (1990) 1

[5] See e.g. J.S.Cohen, Phys.Rev. **A27** (1983) 167

[6] V.E.Markushin, Sov.Phys.JETP **53** (1981) 16

[7] H.Bethe and E.E.Salpeter: "Quantum Mechanics of One- and Two-Electron Systems", in Handbuch der Physik, band XXXV (ATOME I), Springer-Verlag (Berlin 1957)

[8] E.A.Ühling, Phys.Rev. **48** (1935) 55

[9] E.Borie, Z.Phys. **A278** (1976) 127

[10] A.C.Zemach, Phys.Rev. **104** (1956) 1771

[11] A.Maitland and M.H.Dunn: "Laser Physics", (see particularly chapter 3) North-Holland (Amsterdam, 1969)

[12] P.Hauser, in the Proceedings of the "Workshop on Muonic Atoms and Molecules", April 1992, Ascona, Switzerland (to be published)

[13] E.Borie and M.Leon, Phys.Rev. **A21** (1980) 1460

Table 1: Constants

Physical constants	
Rydberg Frequency	$3.28985*10^{15}$ Hz
Rydberg Energy	13.6056981 eV
Proton Mass	938.27231 10^6 eV
Proton Gyromagnetic Ratio	2*2.7928474
Electron Mass	0.51099906 10^6 eV
Muon Mass	105.658387 10^6 eV
α	1/137.0359895
Conversion factors	
Hz to eV	4.13567 10^{-15} eV/Hz
eV to Hz	2.41799 10^{14} Hz/eV
Hz to µm	$3*10^{14}$ Hz*µm
eV to µm	1.2407 eV*µm

Table 2: Binding energies from the Balmer formula

n	energy (eV)
1	−2528.
2	−632.1
3	−280.9
4	−158.0
5	−101.1
6	−70.24
7	-51.60
8	−39.51
9	−31.22
10	−25.28
11	−20.90
12	−17.56
13	−14.96
14	−12.90

Table 3: Electric dipole transition probabilities (n,l)->(n,l±1) per unit time

transition	Γ (10^9 s^{-1})	intensity (erg s^{-1})
2P-1S	129.73	2.12384
3S-2P	1.30738	0.0039636
3P-1S	34.6337	0.671997
3P-2S	4.64845	0.0140928
3D-2P	13.3875	0.0405873
4S-2P	0.533868	0.00218502
4S-3P	0.380069	0.000403291
4P-1S	14.1197	0.288946
4P-2S	2.002	0.00819383
4P-3S	0.634707	0.000673488
4P-3D	0.0719657	0.0000763628
4D-2P	4.27094	0.0174802
4D-3P	1.4573	0.00154635
4F-3D	2.85513	0.00302958
5S-2P	0.26684	0.00122318
5S-3P	0.187338	0.000290793
5S-4P	0.133578	0.0000656051
5P-1S	7.11823	0.149164
5P-2S	1.02467	0.00469703
5P-3S	0.339128	0.000526407
5P-3D	0.0309649	0.000048065
5P-4S	0.152652	0.0000749732
5P-4D	0.0390248	0.0000191666
5D-2P	1.95175	0.00894672
5D-3P	0.702285	0.00109011
5D-4P	0.307667	0.000151107
5D-4F	0.0104524	$5.13359\ 10^{-6}$
5F-3D	0.94056	0.00145997
5F-4D	0.535164	0.00026284
5G-4	0.880929	0.000432658

Table 4: Lifetimes

level	lifetime (ns)
2P	0.008
3S	0.764
3P	0.026
3D	0.075
4S	1.094
4P	0.059
4D	0.175
4F	0.350
5S	1.701
5P	0.115
5D	0.336
5F	0.678
5G	1.135

Table 5: FS, HFS and QED corrections (in meV)

transition	FS	HFS	Ühling	Källen	Total
$2S^1_{1/2}$– $2P^3_{3/2}$	–8.415	–18.82	–226.7	–1.337	–255.2
$2S^1_{1/2}$– $2P^3_{1/2}$	0.0000	–23.53	–226.7	–1.337	–251.5
$2S^3_{1/2}$– $2P^1_{1/2}$	0.0000	14.12	–226.7	–1.337	–213.9
$2S^3_{1/2}$– $2P^3_{3/2}$	–8.415	9.41	–226.7	–1.337	–227.
$2S^3_{1/2}$– $2P^3_{1/2}$	0.0000	4.705	–226.7	–1.337	–223.3
$2S^3_{1/2}$– $2P^5_{3/2}$	–8.415	5.646	–226.7	–1.337	–230.8
$3S^1_{1/2}$– $3P^3_{3/2}$	–2.493	–5.576	–65.67	–0.387	–74.13
$3S^1_{1/2}$– $3P^3_{1/2}$	0.0000	–6.971	–65.67	–0.387	–73.03
$3S^3_{1/2}$– $3P^1_{1/2}$	0.0000	4.182	–65.67	–0.387	–61.87
$3S^3_{1/2}$– $3P^3_{3/2}$	–2.493	2.788	–65.67	–0.387	–65.76
$3S^3_{1/2}$– $3P^3_{1/2}$	0.0000	1.394	–65.67	–0.387	–64.66
$3S^3_{1/2}$– $3P^5_{3/2}$	–2.493	1.673	–65.67	–0.387	–66.88
$3P^1_{1/2}$– $3D^3_{3/2}$	–2.493	–1.673	–6.103	–0.040	–10.31
$3P^3_{3/2}$– $3D^3_{3/2}$	0.0000	–0.2788	–6.103	–0.040	–6.422
$3P^3_{3/2}$– $3D^5_{5/2}$	–0.8311	–0.4461	–6.103	–0.040	–7.42
$3P^3_{3/2}$– $3D^5_{3/2}$	0.0000	–0.948	–6.103	–0.040	–7.091
$3P^3_{1/2}$– $3D^3_{3/2}$	–2.493	1.115	–6.103	–0.040	–7.521
$3P^3_{1/2}$– $3D^5_{3/2}$	–2.493	0.4461	–6.103	–0.040	–8.19
$3P^5_{3/2}$– $3D^3_{3/2}$	0.0000	0.8365	–6.103	–0.040	–5.307
$3P^5_{3/2}$– $3D^5_{5/2}$	–0.8311	0.6692	–6.103	–0.040	–6.305
$3P^5_{3/2}$– $3D^5_{3/2}$	0.0000	0.1673	–6.103	–0.040	–5.976
$3P^5_{3/2}$– $3D^7_{5/2}$	–0.8311	0.239	–6.103	–0.040	–6.735
$4S^1_{1/2}$– $4P^3_{3/2}$	–1.052	–2.353	–27.5	–0.162	–31.06
$4S^1_{1/2}$– $4P^3_{1/2}$	0.0000	–2.941	–27.5	–0.162	–30.6
$4S^3_{1/2}$– $4P^1_{1/2}$	0.0000	1.764	–27.5	–0.162	–25.89
$4S^3_{1/2}$– $4P^3_{3/2}$	–1.052	1.176	–27.5	–0.162	–27.53
$4S^3_{1/2}$– $4P^3_{1/2}$	0.0000	0.5881	–27.5	–0.162	–27.07
$4S^3_{1/2}$– $4P^5_{3/2}$	–1.052	0.7058	–27.5	–0.162	–28.
$4P^1_{1/2}$– $4D^3_{3/2}$	–1.052	–0.7058	–2.62	–0.017	–4.394

Table 5 (ctd.): FS, HFS and QED corrections (in meV)

transition	FS	HFS	Ühling	Källen	Total
$4P^3_{3/2}$– $4D^3_{3/2}$	0.0000	–0.1176	–2.62	–0.017	–2.754
$4P^3_{3/2}$– $4D^5_{5/2}$	-0.3506	–0.1882	–2.62	–0.017	–3.175
$4P^3_{3/2}$– $4D^5_{3/2}$	0.0000	–0.3999	–2.62	–0.017	–3.037
$4P^3_{1/2}$– $4D^3_{3/2}$	–1.052	0.4705	–2.62	–0.017	–3.218
$4P^3_{1/2}$– $4D^5_{3/2}$	–1.052	0.1882	–2.62	–0.017	–3.5
$4P^5_{3/2}$– $4D^3_{3/2}$	0.0000	0.3529	–2.62	–0.017	–2.284
$4P^5_{3/2}$– $4D^5_{5/2}$	–0.3506	0.2823	–2.62	-0.017	–2.705
$4P^5_{3/2}$– $4D^5_{3/2}$	0.0000	0.07058	–2.62	–0.017	–2.566
$4P^5_{3/2}$– $4D^7_{5/2}$	–0.3506	0.1008	–2.62	–0.017	–2.886
$4D^3_{3/2}$– $4F^5_{5/2}$	–0.3506	–0.1008	–0.1066	–0.001	–0.5589
$4D^5_{5/2}$– $4F^5_{5/2}$	0.0000	–0.03025	–0.1066	–0.001	–0.1377
$4D^5_{5/2}$– $4F^7_{7/2}$	–0.1753	–0.05185	–0.1066	–0.001	–0.3346
$4D^5_{5/2}$– $4F^7_{5/2}$	0.0000	–0.1599	–0.1066	–0.001	–0.2673
$4D^5_{3/2}$– $4F^5_{5/2}$	–0.3506	0.1815	–0.1066	–0.001	–0.2766
$4D^5_{3/2}$– $4F^7_{5/2}$	–0.3506	0.05185	–0.1066	–0.001	–0.4062
$4D^7_{5/2}$– $4F^5_{5/2}$	0.0000	0.1512	–0.1066	–0.001	0.04377
$4D^7_{5/2}$– $4F^7_{7/2}$	–0.1753	0.1296	–0.1066	–0.001	–0.1532
$4D^7_{5/2}$– $4F^7_{5/2}$	0.0000	0.02161	–0.1066	–0.001	–0.08586
$4D^7_{5/2}$– $4F^9_{7/2}$	–0.1753	0.03361	–0.1066	–0.001	–0.2492
$5S^1_{1/2}$– $5P^3_{3/2}$	–0.5386	–1.205	–14.03	–0.083	–15.86
$5S^1_{1/2}$– $5P^3_{1/2}$	0.0000	–1.506	–14.03	–0.083	–15.62
$5S^3_{1/2}$– $5P^1_{1/2}$	0.0000	0.9034	–14.03	–0.083	–13.21
$5S^3_{1/2}$– $5P^3_{3/2}$	–0.5386	0.6023	–14.03	–0.083	–14.05
$5S^3_{1/2}$– $5P^3_{1/2}$	0.0000	0.3011	–14.03	–0.083	–13.81
$5S^3_{1/2}$– $5P^5_{3/2}$	–0.5386	0.3614	–14.03	–0.083	–14.29
$5P^1_{1/2}$– $5D^3_{3/2}$	–0.5386	–0.3614	–1.351	–0.009	–2.26
$5P^3_{3/2}$– $5D^3_{3/2}$	0.0000	–0.06023	–1.351	–0.009	–1.42
$5P^3_{3/2}$– $5D^5_{5/2}$	–0.1795	–0.09636	–1.351	–0.009	–1.636

Table 5 (ctd.): FS, HFS and QED corrections (in meV)

transition	FS	HFS	Ühling	Källen	Total
$5P^3_{3/2}$– $5D^5_{3/2}$	0.0000	–0.2048	–1.351	–0.009	–1.565
$5P^3_{1/2}$– $5D^3_{3/2}$	–0.5386	0.2409	–1.351	–0.009	–1.658
$5P^3_{1/2}$– $5D^5_{3/2}$	–0.5386	0.09636	–1.351	–0.009	–1.802
$5P^5_{3/2}$– $5D^3_{3/2}$	0.0000	0.1807	–1.351	–0.009	–1.179
$5P^5_{3/2}$– $5D^5_{5/2}$	–0.1795	0.1445	–1.351	–0.009	–1.395
$5P^5_{3/2}$– $5D^5_{3/2}$	0.0000	0.03614	–1.351	–0.009	–1.324
$5P^5_{3/2}$– $5D^7_{5/2}$	–0.1795	0.05162	–1.351	–0.009	–1.488
$5D^3_{3/2}$– $5F^5_{5/2}$	–0.1795	–0.05162	–0.0605	–0.000	–0.2921
$5D^5_{5/2}$– $5F^5_{5/2}$	0.0000	–0.01549	–0.0605	–0.000	–0.07647
$5D^5_{5/2}$– $5F^7_{7/2}$	–0.08976	–0.02655	–0.0605	–0.000	–0.1773
$5D^5_{5/2}$– $5F^7_{5/2}$	0.0000	–0.08186	–0.0605	–0.000	–0.1428
$5D^5_{3/2}$– $5F^5_{5/2}$	–0.1795	0.09292	–0.0605	–0.000	–0.1476
$5D^5_{3/2}$– $5F^7_{5/2}$	–0.1795	0.02655	–0.0605	–0.000	–0.214
$5D^7_{5/2}$– $5F^5_{5/2}$	0.0000	0.07743	–0.0605	–0.000	0.01645
$5D^7_{5/2}$– $5F^7_{7/2}$	–0.08976	0.06637	–0.0605	–0.000	–0.08438
$5D^7_{5/2}$– $5F^7_{5/2}$	0.0000	0.01106	–0.0605	–0.000	–0.04992
$5D^7_{5/2}$– $5F^9_{7/2}$	–0.08976	0.01721	–0.0605	–0.000	–0.1335
$5F^5_{5/2}$– $5G^7_{7/2}$	–0.08976	–0.01721	–0.0012	–0.000	–0.1082
$5F^7_{7/2}$– $5G^7_{7/2}$	0.0000	–0.006145	–0.0012	–0.000	–0.007404
$5F^7_{7/2}$– $5G^9_{9/2}$	–0.05386	–0.01093	–0.0012	–0.000	–0.06604
$5F^7_{7/2}$– $5G^9_{7/2}$	0.0000	–0.04438	–0.0012	–0.000	–0.04564
$5F^7_{5/2}$– $5G^7_{7/2}$	–0.08976	0.04916	–0.0012	–0.000	–0.04186
$5F^7_{5/2}$– $5G^9_{7/2}$	–0.08976	0.01093	–0.0012	–0.000	–0.0801
$5F^9_{7/2}$– $5G^7_{7/2}$	0.0000	0.04302	–0.0012	–0.000	0.04176
$5F^9_{7/2}$– $5G^9_{9/2}$	–0.05386	0.03824	–0.0012	–0.000	–0.01688
$5F^9_{7/2}$– $5G^9_{7/2}$	0.0000	0.00478	–0.0012	–0.000	0.003521

Table 6: Allowed transitions in order of increasing frequency

transition	$h\nu$	ν	λ
$5F^{9}_{7/2} - 5G^{9}_{7/2}$	0.003521 meV	0.8514 GHz	352372. μm
$5F^{7}_{7/2} - 5G^{7}_{7/2}$	–0.007404 meV	1.79 GHz	167564. μm
$5D^{7}_{5/2} - 5F^{5}_{5/2}$	0.01645 meV	3.977 GHz	75426.9 μm
$5F^{9}_{7/2} - 5G^{9}_{9/2}$	–0.01688 meV	4.081 GHz	73507.5 μm
$5F^{9}_{7/2} - 5G^{7}_{7/2}$	0.04176 meV	10.1 GHz	29710.5 μm
$5F^{7}_{5/2} - 5G^{7}_{7/2}$	–0.04186 meV	10.12 GHz	29640.1 μm
$4D^{7}_{5/2} - 4F^{5}_{5/2}$	0.04377 meV	10.58 GHz	28342.8 μm
$5F^{7}_{7/2} - 5G^{9}_{7/2}$	–0.04564 meV	11.04 GHz	27182.8 μm
$5F^{9}_{7/2} - 5G^{11}_{9/2}$	–0.0473 meV	11.44 GHz	26232.9 μm
$5D^{7}_{5/2} - 5F^{7}_{5/2}$	–0.04992 meV	12.07 GHz	24852.7 μm
$5F^{7}_{7/2} - 5G^{9}_{9/2}$	–0.06604 meV	15.97 GHz	18786.4 μm
$5D^{5}_{5/2} - 5F^{5}_{5/2}$	–0.07647 meV	18.49 GHz	16224.5 μm
$5F^{7}_{5/2} - 5G^{9}_{7/2}$	–0.0801 meV	19.37 GHz	15489.9 μm
$5D^{7}_{5/2} - 5F^{7}_{7/2}$	–0.08438 meV	20.4 GHz	14704.3 μm
$4D^{7}_{5/2} - 4F^{7}_{5/2}$	–0.08586 meV	20.76 GHz	14450.8 μm
$5F^{5}_{5/2} - 5G^{7}_{7/2}$	–0.1082 meV	26.17 GHz	11463.5 μm
$5D^{7}_{5/2} - 5F^{9}_{7/2}$	–0.1335 meV	32.29 GHz	9290.81 μm
$4D^{5}_{5/2} - 4F^{5}_{5/2}$	–0.1377 meV	33.3 GHz	9009.57 μm
$5D^{5}_{5/2} - 5F^{7}_{5/2}$	–0.1428 meV	34.54 GHz	8685.82 μm
$5D^{5}_{3/2} - 5F^{5}_{5/2}$	–0.1476 meV	35.69 GHz	8406.28 μm
$4D^{7}_{5/2} - 4F^{7}_{7/2}$	–0.1532 meV	37.03 GHz	8101.18 μm
$5D^{5}_{5/2} - 5F^{7}_{7/2}$	–0.1773 meV	42.87 GHz	6997.88 μm
$5D^{5}_{3/2} - 5F^{7}_{5/2}$	–0.214 meV	51.74 GHz	5798.66 μm
$4D^{7}_{5/2} - 4F^{9}_{7/2}$	–0.2492 meV	60.25 GHz	4979.26 μm
$4D^{5}_{5/2} - 4F^{7}_{5/2}$	–0.2673 meV	64.64 GHz	4640.9 μm
$4D^{5}_{3/2} - 4F^{5}_{5/2}$	–0.2766 meV	66.89 GHz	4485.25 μm
$5D^{3}_{3/2} - 5F^{5}_{5/2}$	–0.2921 meV	70.64 GHz	4247.03 μm
$4D^{5}_{5/2} - 4F^{7}_{7/2}$	–0.3346 meV	80.91 GHz	3707.63 μm

Table 6 (ctd.): Allowed transitions in order of increasing frequency

transition	$h\nu$	ν	λ
$4D^5_{3/2}$– $4F^7_{5/2}$	–0.4062 meV	98.23 GHz	3054.04 μm
$4D^3_{3/2}$– $4F^5_{5/2}$	–0.5589 meV	135.1 GHz	2219.79 μm
$5P^5_{3/2}$– $5D^3_{3/2}$	–1.179 meV	285.2 GHz	1051.89 μm
$5P^5_{3/2}$– $5D^5_{3/2}$	–1.324 meV	320.2 GHz	937.06 μm
$5P^5_{3/2}$– $5D^5_{5/2}$	–1.395 meV	337.3 GHz	889.292 μm
$5P^3_{3/2}$– $5D^3_{3/2}$	–1.42 meV	343.5 GHz	873.489 μm
$5P^5_{3/2}$– $5D^7_{5/2}$	–1.488 meV	359.8 GHz	833.762 μm
$5P^3_{3/2}$– $5D^5_{3/2}$	–1.565 meV	378.4 GHz	792.811 μm
$5P^3_{3/2}$– $5D^5_{5/2}$	–1.636 meV	395.6 GHz	758.347 μm
$5P^3_{1/2}$– $5D^3_{3/2}$	–1.658 meV	400.9 GHz	748.379 μm
$5P^3_{1/2}$– $5D^5_{3/2}$	–1.802 meV	435.8 GHz	688.363 μm
$5P^1_{1/2}$– $5D^3_{3/2}$	–2.26 meV	546.5 GHz	548.956 μm
$4P^5_{3/2}$– $4D^3_{3/2}$	–2.284 meV	552.2 GHz	543.275 μm
$4P^5_{3/2}$– $4D^5_{3/2}$	–2.566 meV	620.5 GHz	483.506 μm
$4P^5_{3/2}$– $4D^5_{5/2}$	–2.705 meV	654.1 GHz	458.676 μm
$4P^3_{3/2}$– $4D^3_{3/2}$	–2.754 meV	666. GHz	450.467 μm
$4P^5_{3/2}$– $4D^7_{5/2}$	–2.886 meV	697.9 GHz	429.837 μm
$4P^3_{3/2}$– $4D^5_{3/2}$	–3.037 meV	734.2 GHz	408.587 μm
$4P^3_{3/2}$– $4D^5_{5/2}$	–3.175 meV	767.8 GHz	390.714 μm
$4P^3_{1/2}$– $4D^3_{3/2}$	–3.218 meV	778.1 GHz	385.546 μm
$4P^3_{1/2}$– $4D^5_{3/2}$	–3.5 meV	846.4 GHz	354.451 μm
$4P^1_{1/2}$– $4D^3_{3/2}$	–4.394 meV	063. GHz	282.342 μm
$3P^5_{3/2}$– $3D^3_{3/2}$	–5.307 meV	1283. GHz	233.803 μm
$3P^5_{3/2}$– $3D^5_{3/2}$	–5.976 meV	1445. GHz	207.621 μm
$3P^5_{3/2}$– $3D^5_{5/2}$	–6.305 meV	1525. GHz	196.779 μm
$3P^3_{3/2}$– $3D^3_{3/2}$	–6.422 meV	1553. GHz	193.198 μm
$3P^5_{3/2}$– $3D^7_{5/2}$	–6.735 meV	1629. GHz	184.21 μm
$3P^3_{3/2}$– $3D^5_{3/2}$	–7.091 meV	1715. GHz	174.966 μm

Table 6 (ctd.): Allowed transitions in order of increasing frequency

transition	$h\nu$	ν	λ
$3P^3_{3/2}$– $3D^5_{5/2}$	–7.42 meV	1794. GHz	167.203 μm
$3P^3_{1/2}$– $3D^3_{3/2}$	–7.521 meV	1819. GHz	164.96 μm
$3P^3_{1/2}$– $3D^5_{3/2}$	–8.19 meV	1980. GHz	151.482 μm
$3P^1_{1/2}$– $3D^3_{3/2}$	–10.31 meV	2493. GHz	120.346 μm
$5S^3_{1/2}$– $5P^1_{1/2}$	–13.21 meV	3194. GHz	93.9271 μm
$5S^3_{1/2}$– $5P^3_{1/2}$	–13.81 meV	3340. GHz	89.8314 μm
$5S^3_{1/2}$– $5P^3_{3/2}$	–14.05 meV	3397. GHz	88.313 μm
$5S^3_{1/2}$– $5P^5_{3/2}$	–14.29 meV	3455. GHz	86.8242 μm
$5S^1_{1/2}$– $5P^3_{1/2}$	–15.62 meV	3776. GHz	79.4393 μm
$5S^1_{1/2}$– $5P^3_{3/2}$	–15.86 meV	3834. GHz	78.2496 μm
$4S^3_{1/2}$– $4P^1_{1/2}$	–25.89 meV	6261. GHz	47.9146 μm
$4S^3_{1/2}$– $4P^3_{1/2}$	–27.07 meV	6546. GHz	45.8326 μm
$4S^3_{1/2}$– $4P^3_{3/2}$	–27.53 meV	6658. GHz	45.0606 μm
$4S^3_{1/2}$– $4P^5_{3/2}$	–28. meV	6771. GHz	44.3035 μm
$4S^1_{1/2}$– $4P^3_{1/2}$	–30.6 meV	7399. GHz	40.5469 μm
$4S^1_{1/2}$– $4P^3_{3/2}$	–31.06 meV	7511. GHz	39.9416 μm
$3S^3_{1/2}$– $3P^1_{1/2}$	–61.87 meV	14960. GHz	20.0522 μm
$3S^3_{1/2}$– $3P^3_{1/2}$	–64.66 meV	15640. GHz	19.1875 μm
$3S^3_{1/2}$– $3P^3_{3/2}$	–65.76 meV	15900. GHz	18.8668 μm
$3S^3_{1/2}$– $3P^5_{3/2}$	–66.88 meV	16170. GHz	18.5521 μm
$3S^1_{1/2}$– $3P^3_{1/2}$	–73.03 meV	17660. GHz	16.9897 μm
$3S^1_{1/2}$– $3P^3_{3/2}$	–74.13 meV	51710. GHz	5.8011 μm
$2S^3_{1/2}$– $2P^3_{1/2}$	–223.3 meV	53990. GHz	5.55661 μm
$2S^3_{1/2}$– $2P^3_{3/2}$	–227. meV	54890. GHz	5.46579 μm
$2S^3_{1/2}$– $2P^5_{3/2}$	–230.8 meV	55800. GHz	5.37663 μm
$2S^1_{1/2}$– $2P^3_{1/2}$	–251.5 meV	60820. GHz	4.93292 μm

Table 7: Finite size corrections

n	shift (meV)
1	12.9039
2	1.61299
3	0.477923
4	0.201624
5	0.103231

Table 8a: Transition probabilities normalized to source intensity for the 3D-3P transitions

transition	$T(\omega_o)$ $*10^{-13}(W/m^2)^{-1}$
$3P^5_{3/2} - 3D^3_{3/2}$	0.05
$3P^3_{3/2} - 3D^5_{3/2}$	0.5
$3P^3_{3/2} - 3D^5_{5/2}$	0.3
$3P^3_{3/2} - 3D^3_{3/2}$	0.3
$3P^5_{3/2} - 3D^7_{5/2}$	4.2
$3P^3_{3/2} - 3D^5_{3/2}$	0.05
$3P^3_{3/2} - 3D^5_{5/2}$	2.8
$3P^3_{1/2} - 3D^3_{3/2}$	0.5
$3P^3_{1/2} - 3D^5_{3/2}$	2.5
$3P^1_{1/2} - 3D^3_{3/2}$	1.0

Table 8b: Transition probabilities normalized to source intensity for the 4D-4P transitions

transition	$T(\omega_o)$ $*10^{-13}(W/m^2)^{-1}$
$4P^5_{3/2} - 4D^3_{3/2}$	0.2
$4P^5_{3/2} - 4D^5_{3/2}$	1.9
$4P^5_{3/2} - 4D^5_{5/2}$	1.2
$4P^3_{3/2} - 4D^3_{3/2}$	1.0
$4P^5_{3/2} - 4D^7_{5/2}$	17.
$4P^3_{3/2} - 4D^5_{3/2}$	0.2
$4P^3_{3/2} - 4D^5_{5/2}$	11.
$4P^3_{1/2} - 4D^3_{3/2}$	2.1
$4P^3_{1/2} - 4D^5_{3/2}$	10.
$4P^1_{1/2} - 4D^3_{3/2}$	4.1

Table 8c: Transition probabilities normalized to source intensity for the 4S-4P transitions

transition	$T(\omega_o)$ $*10^{-13}(W/m^2)^{-1}$
$4S^3_{1/2} - 4P^1_{1/2}$	2.1
$4S^3_{1/2} - 4P^3_{1/2}$	4.2
$4S^3_{1/2} - 4P^3_{3/2}$	2.1
$4S^3_{1/2} - 4P^5_{3/2}$	1.0
$4S^1_{1/2} - 4P^3_{1/2}$	2.1
$4S^1_{1/2} - 4P^3_{3/2}$	2.1

Table 9: Statistical populations at very low gas pressure

nL	% fraction of μ that pass through level
4S	0.2
4P	3.0
4D	10.
4F	36.
3S	0.6
3P	8.7
3D	54.
2S	2.8
2P	78.

Table 10: Statistical populations of hyperfine sublevels

L_j^{2f+1}	% of total population
$S_{1/2}^1$	25%
$S_{3/2}^1$	75%
$P_{1/2}^1$	8.3%
$P_{1/2}^3$	25%
$P_{3/2}^3$	25%
$P_{3/2}^5$	41.7%
$D_{3/2}^3$	15%
$D_{3/2}^5$	25%
$D_{5/2}^5$	25%
$D_{5/2}^7$	35%